Supporting Information

Byrne et al. 10.1073/pnas.1500161112

SI Methods

Molecular Biology. The coding region of the *E. coli dusC* gene (EcoGene accession no. EG12022; UniProtKB accession no. P33371) was amplified from *E. coli* genomic DNA by PCR and inserted into the vector pET28a (Merck Biosciences). Mutagenesis of Cys98 to Ala was performed using overlap extension PCR (1). DusC (wild-type and C98A mutant) was expressed in Rosetta pLysS (DE3) cells. LB medium was inoculated with cells from a starter culture and incubated at 37 °C until $OD_{600\ nm}$ ~0.6. At this point isopropyl β-D-1-thiogalactopyranoside was added to a final concentration of 1 mM and the cells were incubated at 16 °C for 16 h before harvesting by centrifugation. Selenomethionine DusC was produced in a similar manner using methionine auxotrophic B834 (DE3) cells grown in a minimal medium containing L-selenomethionine (Acros Organics) as detailed in ref. 2.

Protein Purification. Cells were resuspended in buffer A (500 mM NaCl, 20 mM Tris•HCl pH 7.5, 20 mM imidazole, and 5 mM DTT) supplemented with a complete EDTA-free protease inhibitor tablet (Roche) and lysed by sonication. The lysate was clarified by centrifugation, and the soluble fraction was loaded onto a 5-mL HisTrap HP column (GE Healthcare) equilibrated with buffer A. Protein was eluted with a gradient of imidazole (20–500 mM), and fractions containing DusC were pooled and concentrated before dilution with 20 mM Tris•HCl pH 7.5. The pool was loaded onto a 5-mL MonoQ column (GE Healthcare) equilibrated with 50 mM NaCl, 20 mM Tris•HCl pH 7.5, and 5 mM DTT. Bound protein was eluted with a gradient of NaCl (50–1,000 mM). Fractions containing DusC without nucleic acid contaminants were pooled and concentrated. These fractions were loaded onto a Superdex 75 10/300 GL column (GE Healthcare) equilibrated with buffer B (100 mM NaCl, 20 mM Tris•HCl pH 7.5, and 5 mM DTT) for SEC. The resulting protein was concentrated to 10–15 $mg{\bullet}mL^{-1}$. For biochemical and cocrystallization experiments with $tRNA^{Phe}$ and $tRNA^{Trp}$, the hexahistidine tag was removed after the anion-exchange chromatography step. Thrombin was added to DusC at a ratio of four units of thrombin per milligram of DusC, and the mixture was incubated overnight at 4 °C. Digested DusC was isolated by passing the protein through a HisTrap HP column and then further purified with a Superdex 75 column as described above.

SEC and Multiangle Light Scattering. Samples of purified DusC (2 $mg{\bullet}mL^{-1}$) were loaded onto a Biosep SEC S3000 column (Phenomenex) preequilibrated with buffer B connected to a Dawn Helios II 18-angle light-scattering detector (Wyatt Technology). The eluting species was detected by measuring the UV absorbance at 280 nm, the concentration of the species was determined using an Optilab rEX refractometer (Wyatt Technology), and a refractive index increment of 0.18 $mL{\bullet}g^{-1}$ was used for calculation of the molecular weight.

In Vitro $tRNA^{Phe}$ Dihydrouridylation and Dihydrouridine Detection. Unmodified tRNA produced as described previously (3) was refolded by heating and cooling before reaction with enzyme. We incubated 2 μM $tRNA^{Phe}$ without enzyme, or with 1 μM of purified $DusC^{WT}$ or $DusC^{C98A}$ in 100 mM Tris•HCl pH 8, 100 mM NH_4Ac, 5 mM $MgCl_2$, 2 mM DTT, 0.1 mM EDTA, 1 mM β-NADH, 1 mM NADPH, and 250 μM flavin mononucleotide (FMN) in a total volume of 100 μL for 1 h at 37 °C. DusC was removed using phenol extraction and $tRNA^{Phe}$ isolated by ethanol precipitation. Treated $tRNA^{Phe}$ was then resuspended in 9 μL of diethyl pyrocarbonate-treated water.

Dihydrouridine residues incorporated following DusC treatment were subjected to alkaline hydrolysis causing ring-opening to form β-ureidopropionic acid. β-ureidopropionic acid is unable to form base pairs and consequently inhibits elongation by reverse transcriptase (4). Alkaline hydrolysis was performed by addition of 100 mM KOH and incubation for 20 min at 37 °C. The mixture was neutralized by addition of 125 mM Tris•HCl pH 8, 75 mM NaCl, and 25 mM DTT. Treated tRNA was used as a template for reverse transcriptase using a fluorescein (FAM)-labeled primer specific for the 3′ end of $tRNA^{Phe}$. We used 0.6 μg of tRNA and 5 nM of FAM-labeled primer complementary to $tRNA^{Phe}$ (5′ FAM-GCCCGGACTCGGAATCGAAC 3′) in a reverse transcription primer extension reaction as per the manufacturer's instruction (Invitrogen SuperScript III Reverse Transcriptase). A reverse transcription enrichment step was included to enhance product concentration (5). Reverse transcript fragments were purified by ethanol precipitation, and a dilution series was prepared and separated by capillary electrophoresis. Diluted fragments were mixed with 0.3 μL of Genescan 600 LIZ size standards before loading on an AB3130XL instrument (Applied Biosystems) using default parameters. Results were analyzed using Genemapper software v4.0 (Applied Biosystems) default amplified fragment-length polymorphism analysis in the size range 25–70, normalized to total fluorescence. Capillary electrophoresis achieved separation of full-length and termination products with single nucleotide resolution. Enhanced termination of primer extension at position *n* of the tRNA indicates that extension beyond this point was prevented due to the presence of β-ureidopropionic acid (and therefore dihydrouridine) at position *n* – *1* with respect to the 5′–3′ sequence of the tRNA. The data presented are representative of replicate experiments that identified the same reverse transcript termination products.

Electrophoretic Mobility Shift Assays. Unmodified $tRNA^{Phe}$ was refolded by heating and cooling before mixing with enzyme. $tRNA^{Phe}$ (8.3 μM) was incubated at 37 °C for 30 min in the absence or presence of a 1:1, 1:2, or 1:4 molar ratio of $DusC^{WT}$ or $DusC^{C98A}$ in buffer comprising 50 mM Tris pH 7.5, 20 mM NaCl, 5 mM $MgCl_2$, 8% glycerol, and 5 mM DTT. A 1.5-mm 10% (wt/vol) native PAGE gel was prepared with Tris/Borate buffer at pH 8.5 with the addition of 2% glycerol and 5 mM $MgCl_2$. The gel was prerun at 80 V for 30 min at 4 °C. $tRNA^{Phe}$, $DusC^{WT}$, $DusC^{C98A}$, and the mixed ratios described above were loaded and electrophoresed at 80 V for 150 min at 4 °C. The gel was stained using SYBR-Gold nucleic acid gel stain (Invitrogen) diluted in running buffer 1/10,000 with rocking at room temperature for 20 min. The gel was destained in running buffer for 20 min at room temperature and UV imaged before Coomassie staining by standard methods.

Analytical SEC. Deacylated unmodified $tRNA^{Trp}$ (135 pmol) or $tRNA^{Cys}$ (190 pmol) was mixed with an excess of $DusC^{C98A}$ (250 pmol) or $DusC^{WT}$ (500 pmol) in 50 mM Tris•HCl buffer (pH 7.5) containing 7 mM $MgCl_2$, 50 mM KCl, and 70 mM NH_4Cl. After 10 min of incubation at 25 °C, 200 μL of sample was injected and the complex was analyzed by SEC using a Biosuite 250 5 μm HR 7.8 × 300 column on a Waters Alliance HPLC system. Nucleic acid was detected by absorbance at 260 nm, and protein was detected by tryptophan fluorescence (λ_{ex} = 280 nm and λ_{em} = 320 nm) using UV/V is 2487 and Fluorescence 2475 HPLC detectors (Waters).

Crystallization of DusC. DusC was crystallized in MRC Crystallization Plates (Swissci AG) at 20 °C. Protein (150 nL) at a concentration of

10–15 mg•mL^{-1} in 100 mM NaCl, 20 mM Tris-HCl pH 7.5, and 5 mM DTT was mixed with 150 nL of the crystallization condition and equilibrated against a 56-μL reservoir of the crystallization condition. Crystals of native DusC grew over a period of 8 wk in condition C10 [10% (wt/vol) PEG 8000, 20% (vol/vol) ethylene glycol, 0.1 M Bicine/Tris pH 8.5, and 30 mM each of $NaNO_3$, Na_2HPO_4, and $(NH_4)_2SO_4$] of the Morpheus screen (6). Crystals of the selenomethionine derivative grew in 3 d in condition D3 [10% (wt/vol) PEG 4000, 20% (wt/vol) glycerol, 0.1 M Mes/imidazole pH 6.5, and 20 mM each of 1,6-hexanediol, 1-butanol, (RS)-1,2-propanediol, 2-propanol, 1,4-butanediol, and 1,3-propanediol] of the Morpheus screen. All crystals were flash-cooled in liquid nitrogen straight from the drop.

Crystallization of DusC^{C98A}–tRNA^{Phe} Complex. The DusC^{C98A}–tRNA^{Phe} complex was formed by mixing DusC^{C98A} and tRNA^{Phe} in a 1:1 molar ratio, following buffer exchange of the protein into a solution containing 100 mM $MgCl_2$ and 10 mM Hepes-NaOH pH 7.0 using a 0.5-mL Vivaspin 10 kDa MWCO concentrator. Protein concentration in the final complex was 7.5 mg•mL^{-1}. Complex (1 μL) was mixed with 1 μL of the reservoir solution containing 100 mM Hepes pH 7.0, 200 mM $MgCl_2$, 10 mM $MnCl_2$, and 11% (wt/vol) PEG 6K and equilibrated over 1 mL of reservoir. Crystals grew over the course of 3 d at 20 °C. Before vitrification, crystals were transferred into a solution containing 100 mM Hepes pH 7.0, 150 mM $MgCl_2$, 10 mM $MnCl_2$, 18% (wt/vol) PEG 6K, and 15% (vol/vol) glycerol.

Crystallization of DusC^{C98A}–tRNA^{Trp} Complex. *E. coli* tRNA^{Trp} transcript in 20 mM Hepes pH 7.5, 5 mM $MgCl_2$ was refolded by heating to 60 °C for 10 min followed by cooling to room temperature at a rate of 0.1 °C/s. DusC^{C98A} was then added in a 1:1 molar ratio. Crystals grew after ∼6 mo in sitting drops (0.5 μL) equilibrated against 0.1 M Bis•Tris pH 6.5, 0.2 M Li_2SO_4, and 22–28% (wt/vol) PEG monomethyl ether 2,000. Crystals were cryoprotected by addition of a solution containing 0.1 M Bis•Tris pH 6.5, 0.2 M Li_2SO_4, 30% (wt/vol) PEG monomethyl ether 2,000, and 10% (vol/vol) glycerol.

Structure Determination. X-ray data were collected at Diamond Light Source (Didcot) beamlines I02, I04, and I24. Two datasets were collected from crystals of DusC alone: a dataset from an orthorhombic crystal of native DusC (crystal 1) and a dataset from a tetragonal crystal of selenomethionine DusC (crystal 2) at the peak wavelength of 0.9808 Å. Two datasets were collected from a single crystal of the DusC–tRNA^{Phe} complex (crystal 3) at two different wavelengths: 0.9795 Å data for structure refinement and longer wavelength data (1.300 Å) for identification of Mn^{2+} ion positions. A single dataset was collected from a single crystal of the DusC–tRNA^{Trp} complex (crystal 4). After integration with iMosflm (7) (crystals 1 and 2) or XDS (8) (crystals 3 and 4), the data were imported into the CCP4 suite (9). The data were analyzed with Pointless, scaled and merged with Scala (10) (crystals 1 and 2) or merged with Aimless (11) (crystals 3 and 4), and the resulting intensities were converted to amplitudes with cTruncate (Table 1).

The structure of selenomethionine DusC (crystal 2) was determined by single wavelength anomalous diffraction. The selenium positions were located by SHELXC and SHELXD (12), refined by Phaser (13), and the resulting phases were improved by density modification with Parrot (14). The single molecule of selenomethionine DusC present in the asymmetric unit was automatically built by Buccaneer (15). The model was further improved through alternate cycles of manual rebuilding with Coot (16) and refinement with Refmac5 (17) using an isotropic *B* factor for each atom and two TLS (18) groups as suggested by the TLSMD server (19). Restraints for FMN were created with GRADE (20). The FMN cofactor and all residues of DusC (including three preceding vector-derived residues) are clearly defined in the electron density maps. The final model contains one molecule of selenomethionine DusC, one molecule of FMN, and 104 water molecules (Table 1).

The structure of native DusC (crystal 1) was determined by molecular replacement by Phaser (13) using the structure of selenomethionine DusC as a search model. The model was refined as above, except with the use of anisotropic atomic *B* factors. The final model contains two molecules of DusC, two molecules of FMN, and 611 water molecules.

The structure of the DusC^{C98A}–tRNA^{Phe} complex (crystal 3) was determined by molecular replacement with Phaser (13) using the structures of DusC [Protein Data Bank (PDB) ID code 4bfa] with the FMN cofactor removed and the structure of tRNA^{Phe} transcript (PDB ID code 3l0u). Three molecules each of DusC^{C98A} and tRNA^{Phe} were found in the asymmetric unit, and these were rebuilt and refined using isotropic atomic *B* factors and 21 TLS groups identified by TLSMD (19). FMN molecules were built into clear positive density in the mF_o-DF_c electron density map that corresponded to the FMN cofactor in the structure of DusC. Toward the end of model building and refinement, water molecules were added using ARP/wARP (21), and tRNA geometry was improved using RCrane (22). Mg^{2+} ions were identified as peaks above 6 σ in the mF_o-DF_c difference electron density maps, where coordinating distances were in agreement with those expected for Mg^{2+} ions. To identify Mn^{2+} ion positions, the data collected at a wavelength of 1.300 Å were analyzed by ANODE (23), and inspection of the resulting anomalous difference map revealed the locations of three Mn^{2+} ions, one per molecule of tRNA. The final model contains three DusC^{C98A}–tRNA^{Phe} complexes, three molecules of FMN, 25 Mg^{2+} ions, three Mn^{2+} ions, and 614 water molecules. The DusC^{C98A} and tRNA^{Phe} models are complete, except for amino acids 101–104 (chains A–C), 313–315 (chain B), and 315 (chains A and C) and nucleotides 75–76 (chain D), 1–2 and 70–76 (chain E), and 72–76 (chain F).

The structure of the DusC^{C98A}–tRNA^{Trp} complex (crystal 4) was determined by molecular replacement with Phaser (13) using the structure of DusC (PDB ID code 4bfa) with the FMN cofactor removed. Clear density for tRNA^{Trp} enabled manual building of the majority of the RNA. The density for the anticodon loop, the end of the acceptor stem, and two nucleotides in the variable loop was very poor, and so these regions were not modeled. The RNA geometry was improved using ERRASER (24). The structure was refined using isotropic atomic *B* factors and nine TLS groups identified by TLSMD (19). The final model contains one DusC^{C98A}–tRNA^{Trp} complex, one molecule of FMN, one Mg^{2+} ion, two SO_4 ions, and 52 water molecules. The DusC^{C98A} and tRNA^{Trp} models are complete, except for amino acids 100–106 and nucleotides 1–4, 33–35, 45, 47, and 70–76.

Molecular interfaces were analyzed with PISA (25). The geometry of all models was assessed by MolProbity (26). Figures were created with ccp4mg (27) and PyMol (28). Models were prepared for electrostatic calculations using PDB2PQR (29), and calculations were performed using APBS (30). Multiple sequence alignments were created with Clustal Omega (31) and ESPript (32).

1. Ho SN, Hunt HD, Horton RM, Pullen JK, Pease LR (1989) Site-directed mutagenesis by overlap extension using the polymerase chain reaction. *Gene* 77(1):51–59.
2. Ramakrishnan V, Finch JT, Graziano V, Lee PL, Sweet RM (1993) Crystal structure of globular domain of histone H5 and its implications for nucleosome binding. *Nature* 362(6417):219–223.
3. Byrne RT, Konevega AL, Rodnina MV, Antson AA (2010) The crystal structure of unmodified tRNAPhe from Escherichia coli. *Nucleic Acids Res* 38(12):4154–4162.
4. Xing F, Hiley SL, Hughes TR, Phizicky EM (2004) The specificities of four yeast dihydrouridine synthases for cytoplasmic tRNAs. *J Biol Chem* 279(17):17850–17860.

5. Lloyd AL, Marshall BJ, Mee BJ (2005) Identifying cloned *Helicobacter pylori* promoters by primer extension using a FAM-labelled primer and GeneScan analysis. *J Microbiol Methods* 60(3):291–298.
6. Gorrec F (2009) The MORPHEUS protein crystallization screen. *J Appl Cryst* 42(Pt 6): 1035–1042.
7. Leslie AGW, Powell HR (2007) *Evolving Methods for Macromolecular Crystallography* (Springer, Dordrecht, The Netherlands).
8. Kabsch W (2010) Xds. *Acta Crystallogr D Biol Crystallogr* 66(Pt 2):125–132.
9. Winn MD, et al. (2011) Overview of the CCP4 suite and current developments. *Acta Crystallogr D Biol Crystallogr* 67(Pt 4):235–242.
10. Evans P (2006) Scaling and assessment of data quality. *Acta Crystallogr D Biol Crystallogr* 62(Pt 1):72–82.
11. Evans PR, Murshudov GN (2013) How good are my data and what is the resolution? *Acta Crystallogr D Biol Crystallogr* 69(Pt 7):1204–1214.
12. Sheldrick GM (2008) A short history of SHELX. *Acta Crystallogr A* 64(Pt 1):112–122.
13. McCoy AJ, et al. (2007) Phaser crystallographic software. *J Appl Cryst* 40(Pt 4): 658–674.
14. Cowtan K (2010) Recent developments in classical density modification. *Acta Crystallogr D Biol Crystallogr* 66(Pt 4):470–478.
15. Cowtan K (2006) The Buccaneer software for automated model building. 1. Tracing protein chains. *Acta Crystallogr D Biol Crystallogr* 62(Pt 9):1002–1011.
16. Emsley P, Lohkamp B, Scott WG, Cowtan K (2010) Features and development of Coot. *Acta Crystallogr D Biol Crystallogr* 66(Pt 4):486–501.
17. Murshudov GN, Vagin AA, Dodson EJ (1997) Refinement of macromolecular structures by the maximum-likelihood method. *Acta Crystallogr D Biol Crystallogr* 53(Pt 3): 240–255.
18. Winn MD, Isupov MN, Murshudov GN (2001) Use of TLS parameters to model anisotropic displacements in macromolecular refinement. *Acta Crystallogr D Biol Crystallogr* 57(Pt 1):122–133.
19. Painter J, Merritt EA (2006) TLSMDweb server for the generation of multi-group TLS models. *J Appl Cryst* 39(1):109–111.
20. Smart OS, et al. (2012) *Grade*. Available at grade.globalphasing.org.
21. Langer G, Cohen SX, Lamzin VS, Perrakis A (2008) Automated macromolecular model building for X-ray crystallography using ARP/wARP version 7. *Nat Protoc* 3(7):1171–1179.
22. Keating KS, Pyle AM (2012) RCrane: Semi-automated RNA model building. *Acta Crystallogr D Biol Crystallogr* 68(Pt 8):985–995.
23. Thorn A, Sheldrick GM (2011) ANODE: Anomalous and heavy-atom density calculation. *J Appl Cryst* 44(Pt 6):1285–1287.
24. Chou FC, Sripakdeevong P, Dibrov SM, Hermann T, Das R (2013) Correcting pervasive errors in RNA crystallography through enumerative structure prediction. *Nat Methods* 10(1):74–76.
25. Krissinel E, Henrick K (2007) Inference of macromolecular assemblies from crystalline state. *J Mol Biol* 372(3):774–797.
26. Chen VB, et al. (2010) MolProbity: All-atom structure validation for macromolecular crystallography. *Acta Crystallogr D Biol Crystallogr* 66(Pt 1):12–21.
27. Potterton L, et al. (2004) Developments in the CCP4 molecular-graphics project. *Acta Crystallogr D Biol Crystallogr* 60(Pt 12 Pt 1):2288–2294.
28. Schrödinger, LLC. (2014) The PyMOL Molecular Graphics System (Schrödinger, LLC.), Version 1.7.4.
29. Dolinsky TJ, Nielsen JE, McCammon JA, Baker NA (2004) PDB2PQR: An automated pipeline for the setup of Poisson-Boltzmann electrostatics calculations. *Nucleic Acids Res* 32(web server issue):W665–W667.
30. Baker NA, Sept D, Joseph S, Holst MJ, McCammon JA (2001) Electrostatics of nanosystems: Application to microtubules and the ribosome. *Proc Natl Acad Sci USA* 98(18):10037–10041.
31. Sievers F, et al. (2011) Fast, scalable generation of high-quality protein multiple sequence alignments using Clustal Omega. *Mol Syst Biol* 7:539.
32. Gouet P, Courcelle E, Stuart DI, Métoz F (1999) ESPript: Analysis of multiple sequence alignments in PostScript. *Bioinformatics* 15(4):305–308.

A

Mature *E. coli* tRNAs with D at position 16

	D-loop																	T stem loop																	
Position	10	11	12	13	14	15	16	17	18	19	20	20A	20B	21	22	23	24	50	51	52	53	54	55	56	57	58	59	60	61	62	63	64	65	66
Asn_QUU	G	U	U	C	A	G	D	C	G	G	D	-	-	A	G	A	A	C	U	G	G	T	P	C	G	A	G	U	C	C	A	G	U	C
Asp_QUC	G	U	U	C	A	G	D	C	G	G	D	D	-	A	G	A	A	C	G	G	G	T	P	C	G	A	G	U	C	C	C	G	P	C
Gly_GCC	G	C	U	C	A	G	D	D	G	G	D	-	-	A	G	A	G	C	G	A	G	T	P	C	G	A	G	U	C	U	C	G	U	U
His_QUG	G	C	U	C	A	G	D	D	G	G	D	-	-	A	G	A	G	U	G	G	G	T	P	C	G	A	A	U	C	C	C	A	U	U
Leu_BAA	G	C	G	A	A	A	D	C	#	G	D	A	-	G	A	C	A	C	C	G	G	T	P	C	G	A	G	U	C	C	G	G	C	C
Leu_CAG	G	C	G	G	A	A	D	D	#	G	D	A	-	G	A	C	G	G	G	G	G	T	P	C	A	A	G	U	C	C	C	C	C	C
Leu_GAG	G	U	G	G	A	A	D	D	#	G	D	A	-	G	A	C	A	C	G	G	G	T	P	C	A	A	G	U	C	C	C	G	U	C
Leu_HAA	G	U	G	G	A	A	D	C	#	G	D	A	-	G	A	C	A	C	G	G	G	T	P	C	A	A	G	U	C	C	C	G	C	U
Lys_SUU	G	C	U	C	A	G	D	D	G	G	D	-	-	A	G	A	G	C	A	G	G	T	P	C	G	A	A	U	C	C	U	G	C	A
Met_MAU	G	C	U	C	A	G	D	D	#	G	D	D	-	A	G	A	G	C	A	G	G	T	P	C	G	A	A	U	C	C	C	G	U	C
Phe_GAA	G	C	U	C	A	G	D	C	G	G	D	-	-	A	G	A	G	U	U	G	G	T	P	C	G	A	U	U	C	C	G	A	G	U
Thr_GGU	G	C	U	C	A	G	D	D	G	G	D	-	-	A	G	A	G	G	C	A	G	T	P	C	G	A	A	U	C	U	G	C	C	U
Thr_GGU	G	C	U	C	A	G	D	D	G	G	D	-	-	A	G	A	G	C	C	A	G	T	P	C	G	A	C	U	C	U	G	G	G	U
Trp_CCA	G	U	U	C	A	A	D	D	G	G	D	-	-	A	G	A	G	G	G	A	G	T	P	C	G	A	G	U	C	U	C	U	C	C
Val_GAC	G	C	U	C	A	G	D	D	G	G	D	D	-	A	G	A	G	G	U	G	G	T	P	C	G	A	G	U	C	C	A	C	U	C
Val_GAC	G	C	U	C	A	G	D	D	G	G	D	D	-	A	G	A	G	U	U	G	G	T	P	C	G	A	G	U	C	C	A	A	U	U
A	0	0	0	1	16	5	0	0	0	0	0	4	0	12	4	12	5	0	2	4	0	0	0	0	3	16	4	0	0	0	3	3	0	1
C	0	11	0	12	0	0	0	5	0	0	0	0	0	0	0	4	0	9	3	0	0	0	0	16	0	0	1	0	16	12	8	3	6	8
G	16	0	4	3	0	11	0	0	11	16	0	0	0	4	12	0	11	4	7	12	16	0	0	0	13	0	10	0	0	0	4	9	2	0
U	0	5	12	0	0	0	0	0	0	0	0	0	0	0	0	0	0	3	4	0	0	0	0	0	0	0	1	16	0	4	1	1	7	7
Modified	0	0	0	0	0	0	16	11	5	0	16	4	0	0	0	0	0	0	0	0	0	16	16	0	0	0	0	0	0	0	0	0	1	0
Consensus				C	A	G	D	D			D			A		A	G						P	C											

B

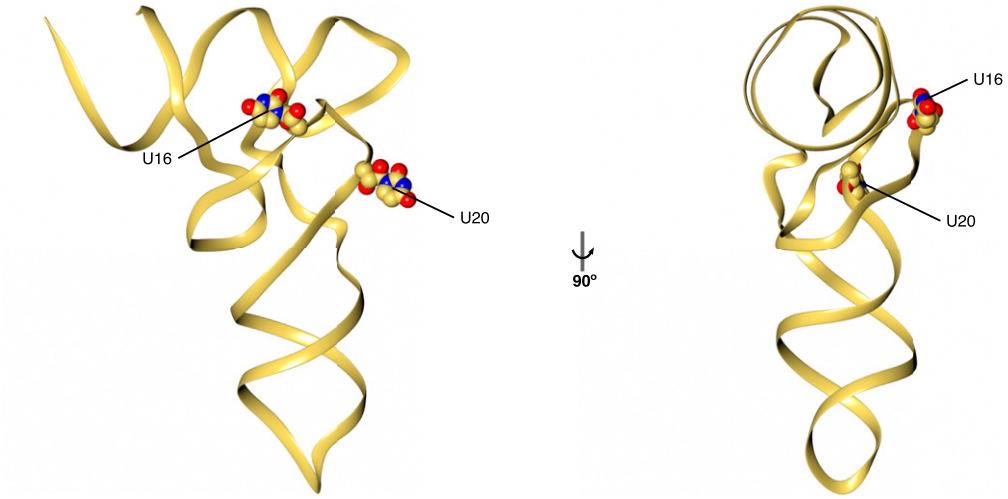

Fig. S1. Dihydrouridine locations in *E. coli* tRNAs. (*A*) Secondary structure-based sequence alignment of mature *E. coli* tRNAs containing dihydrouridine at position 16. DusC forms sequence-specific interactions with positions 16, 17, and 56 (highlighted in dark green) and sequence-independent interactions with positions 13–15, 20, 21, 23–24, and 55 (highlighted in pale green). The consensus row contains the most frequently represented nucleoside at each position. Noncanonical nucleosides are denoted as follows: D, dihydrouridine; *P*, pseudouridine; #, 2′-O-methylguanosine. (*B*) Location of U16 and U20 in unmodified *E. coli* $tRNA^{Phe}$ (PDB ID code 3l0u).

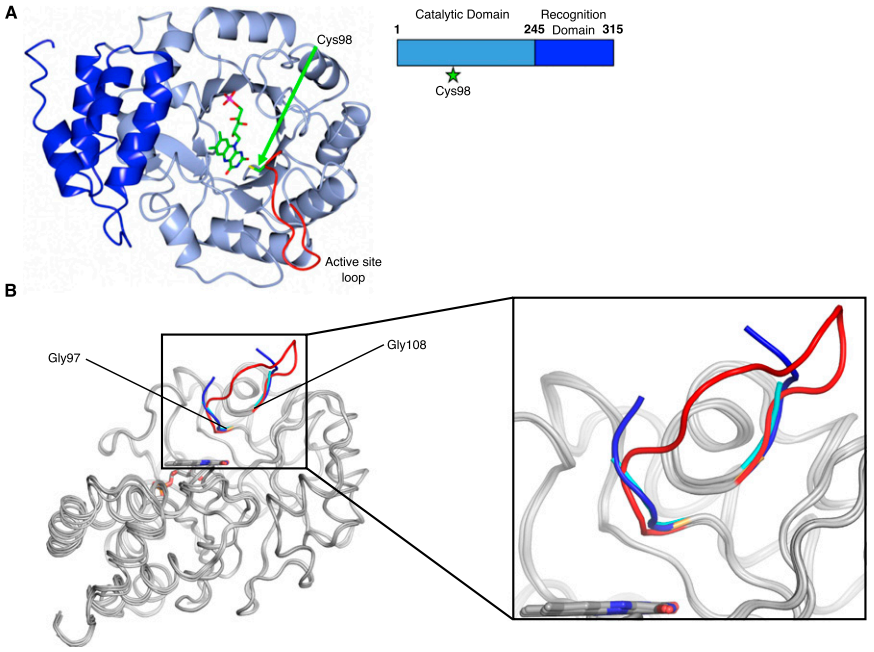

Fig. S2. Active site of DusC. (*A*) The enzyme comprises an N-terminal triosephosphate isomerase barrel domain (1–245, light blue) and C-terminal recognition domain (246–315, blue). FMN cofactor (green sticks) is bound at the center of the TIM barrel. Proximal to this is the active site loop (red) containing the catalytically important cysteine C98 (green). (*B*) Variation in the active site loop positions in structures of DusC (red and yellow), DusC^{C98A}:tRNA^{Phe} complex (blue), and DusC^{C98A}:tRNA^{Trp} complex (cyan).

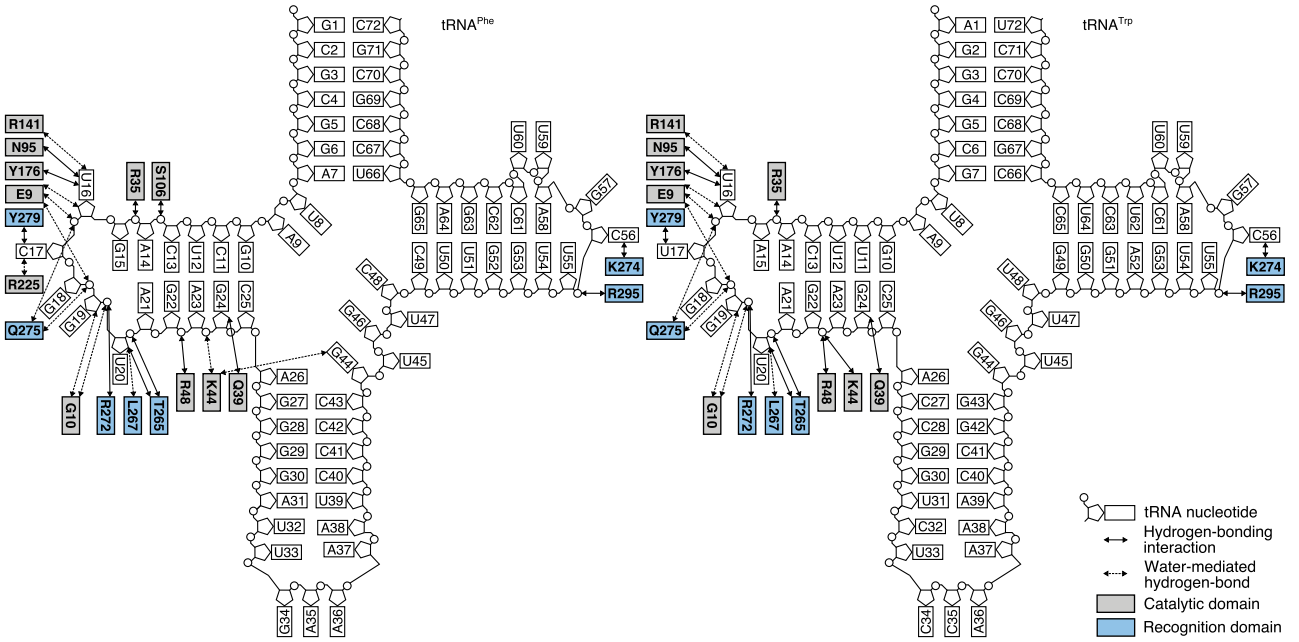

Fig. S3. Schematic of residues hydrogen-bonded to tRNA through direct (solid lines) and water-mediated (dashed lines) contacts in the two DusC:tRNA complexes.

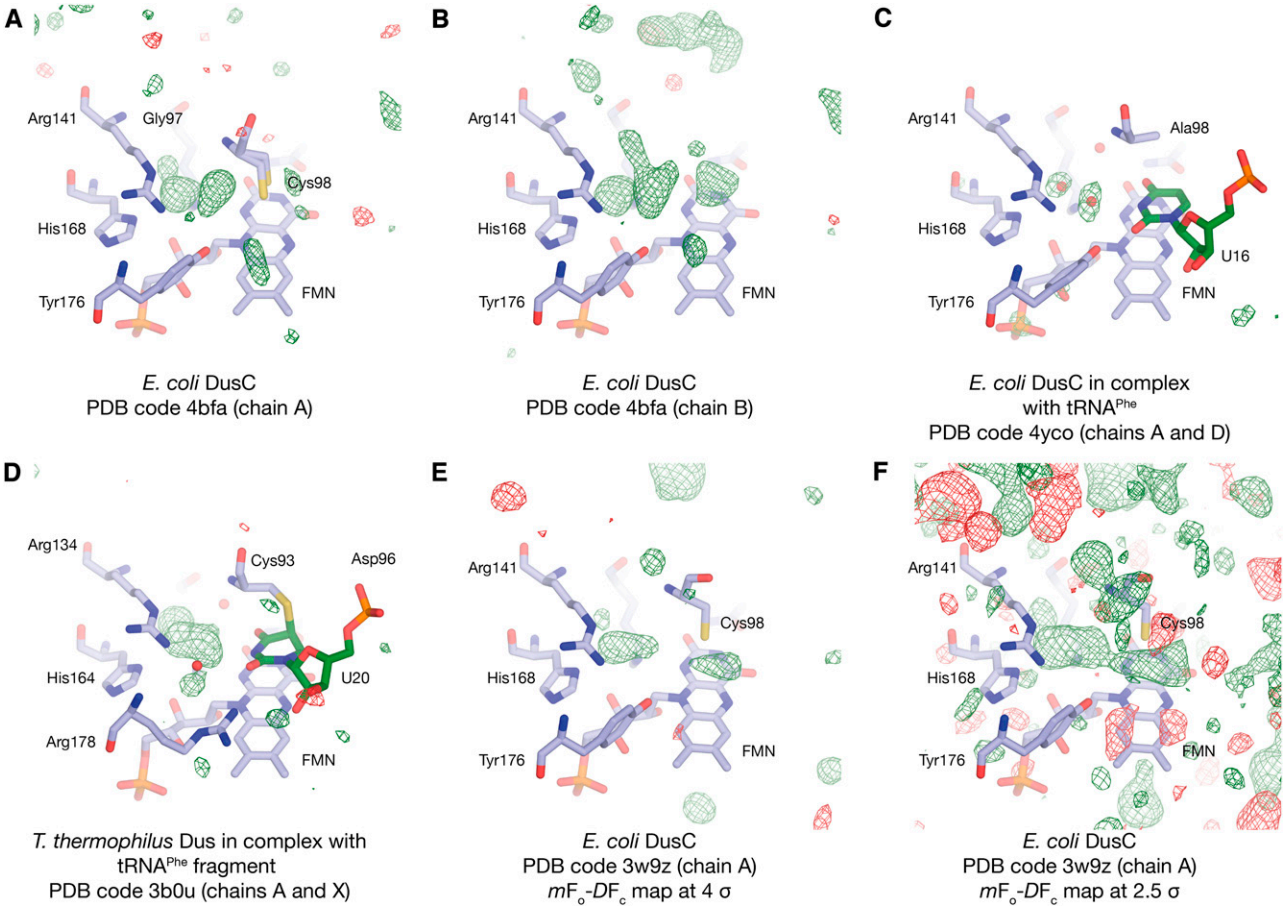

Fig. S4. Difference electron density maps for the active sites of DusC and *Tt*Dus. Positive (green) and negative (red) mF_o-DF_c difference density maps, calculated by PHENIX.MAPS, are contoured at 4 σ. Maps are not clipped around any of the displayed atoms. (*A* and *B*) Structure of DusC (this work, PDB ID code 4bfa; chains A and B). (*C*) Structure of DusC in complex with $tRNA^{Phe}$ (this work). Map is calculated after omitting active site solvent molecules (PDB ID code 4yco; chains A and D). (*D*) Structure of *Tt*Dus in complex with a fragment of $tRNA^{Phe}$ (1) (PDB ID code 3b0u; chains A and X). (*E* and *F*) Structure of DusC from Chen et al. (2) (PDB ID code 3w9z; chain A). Maps were contoured at 4 σ (*E*) and 2.5 σ (*F*). Shape and positional differences in the additional density previously ascribed to an unknown ligand (1, 2) indicate that the additional density may instead correspond to disordered solvent molecules, alternative conformations of the active site loop (residues 96–100), or partially occupied ions and/or polar crystallization ingredients that were brought to the active site by Coulombic attraction.

1. Yu F, et al. (2011) Molecular basis of dihydrouridine formation on tRNA. *Proc Natl Acad Sci USA* 108(49):19593–19598.
2. Chen M, et al. (2013) Structure of dihydrouridine synthase C (DusC) from *Escherichia coli*. *Acta Crystallogr Sect F Struct Biol Cryst Commun* 69(Pt 8):834–838.

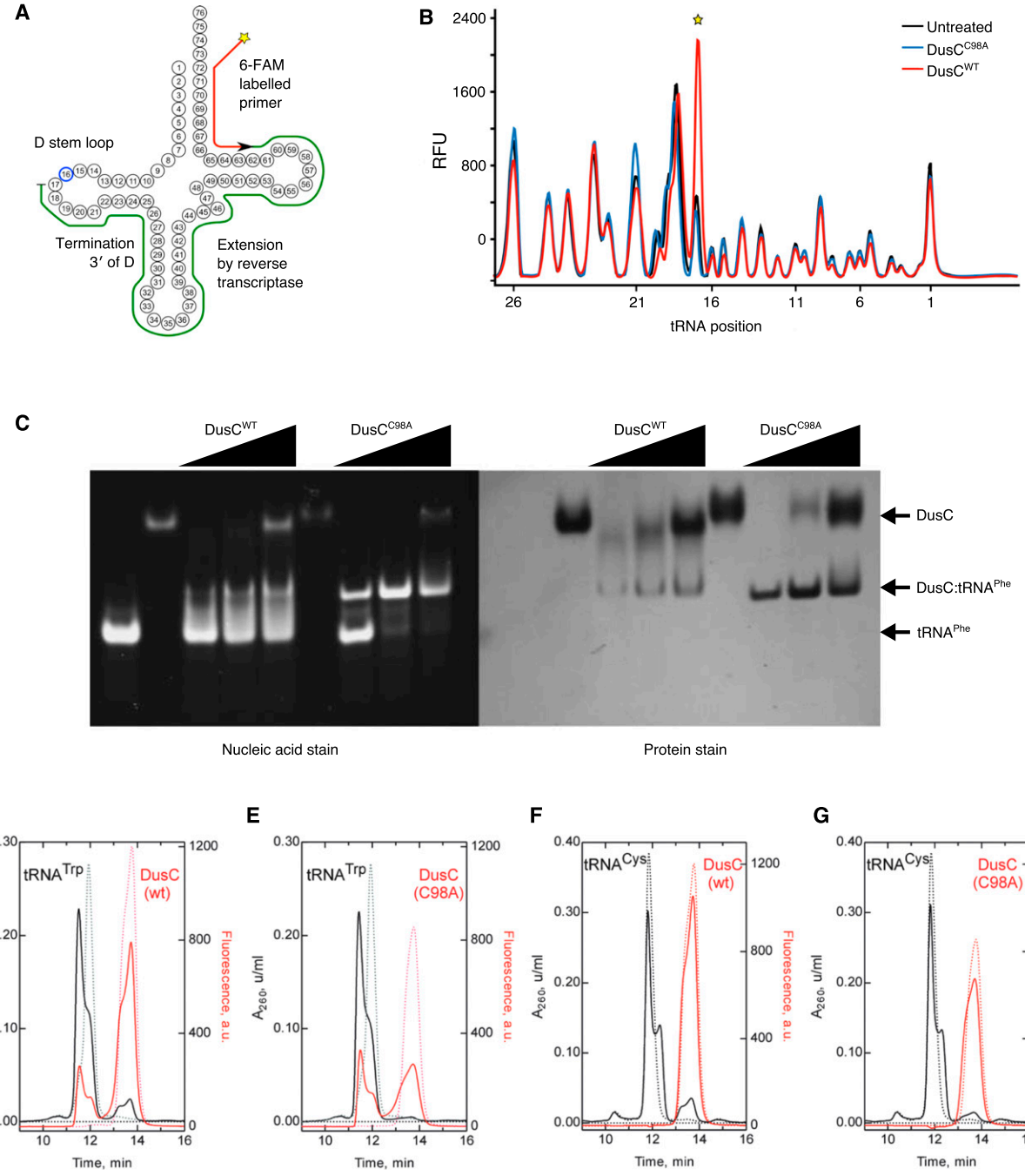

Fig. S5. tRNA binding and modification specificity of *Ec*DusC. (*A*) Reverse transcription assay for dihydrouridine incorporation. (*B*) Capillary fragment analysis of reverse transcript products of unmodified $tRNA^{Phe}$ (black), incubated with 1 μM $DusC^{WT}$ (red), or 1 μM $DusC^{C98A}$ (blue). (*C*) EMSA analysis of $DusC^{WT}$:$tRNA^{Phe}$ and $DusC^{C98A}$:$tRNA^{Phe}$ complex formation. (*D*–*G*) SEC analysis of DusC interactions with unmodified *E. coli* tRNAs. Unmodified $tRNA^{Trp}$ was incubated with $DusC^{WT}$ (*D*) or $DusC^{C98A}$ (*E*), and the DusC–$tRNA^{Trp}$ complex was separated by gel filtration. tRNA was detected by A_{260} (black), and the protein was detected by Trp fluorescence (red). tRNA alone (A_{260}, black dotted line) and DusC alone (fluorescence, red dotted line) controls were separated under identical conditions. Complex formation of $tRNA^{Cys}$ with $DusC^{WT}$ (*F*) or $DusC^{C98A}$ (*G*) was studied in the same way.

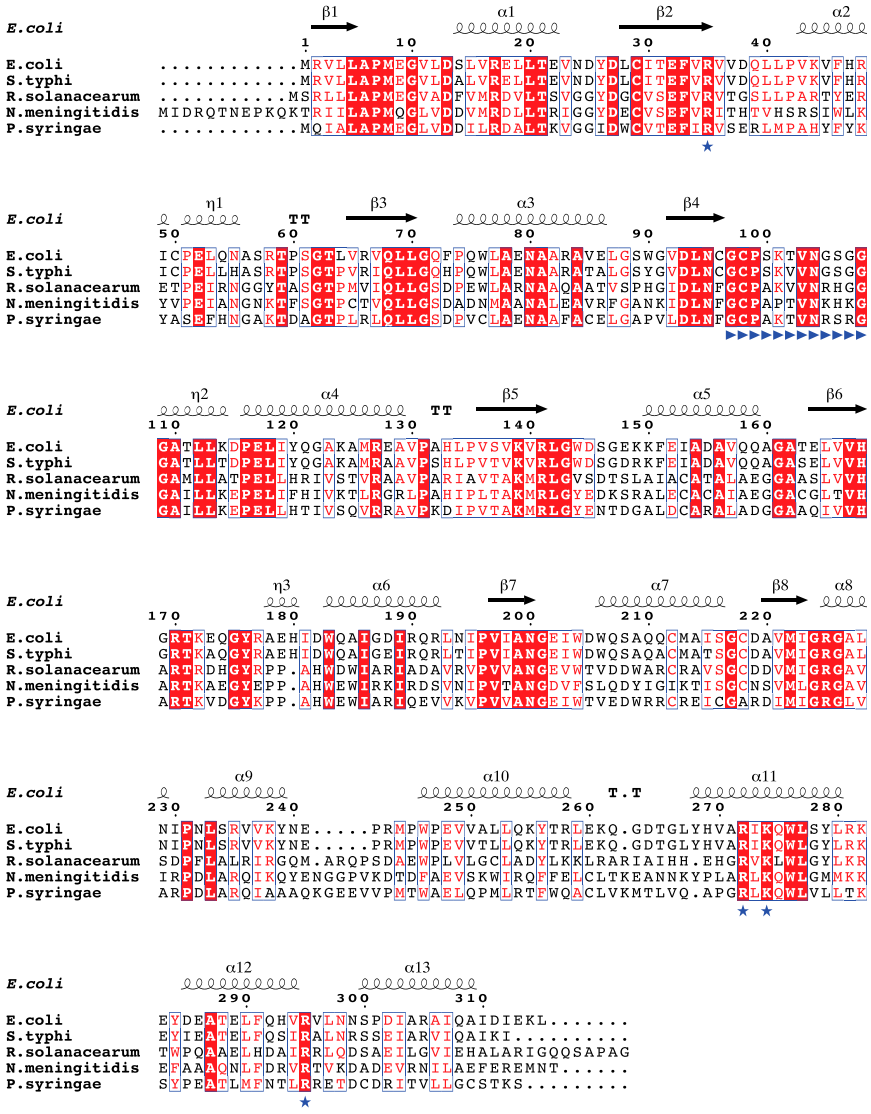

Fig. S6. Sequence alignment of DusC subfamily enzymes with 30–50% sequence identity. Residues that are proposed to define tRNA docking (binding signatures) are highlighted by blue stars. The secondary structure of *Ec*DusC is shown above the sequence alignment. The flexible loop is indicated with blue arrows.

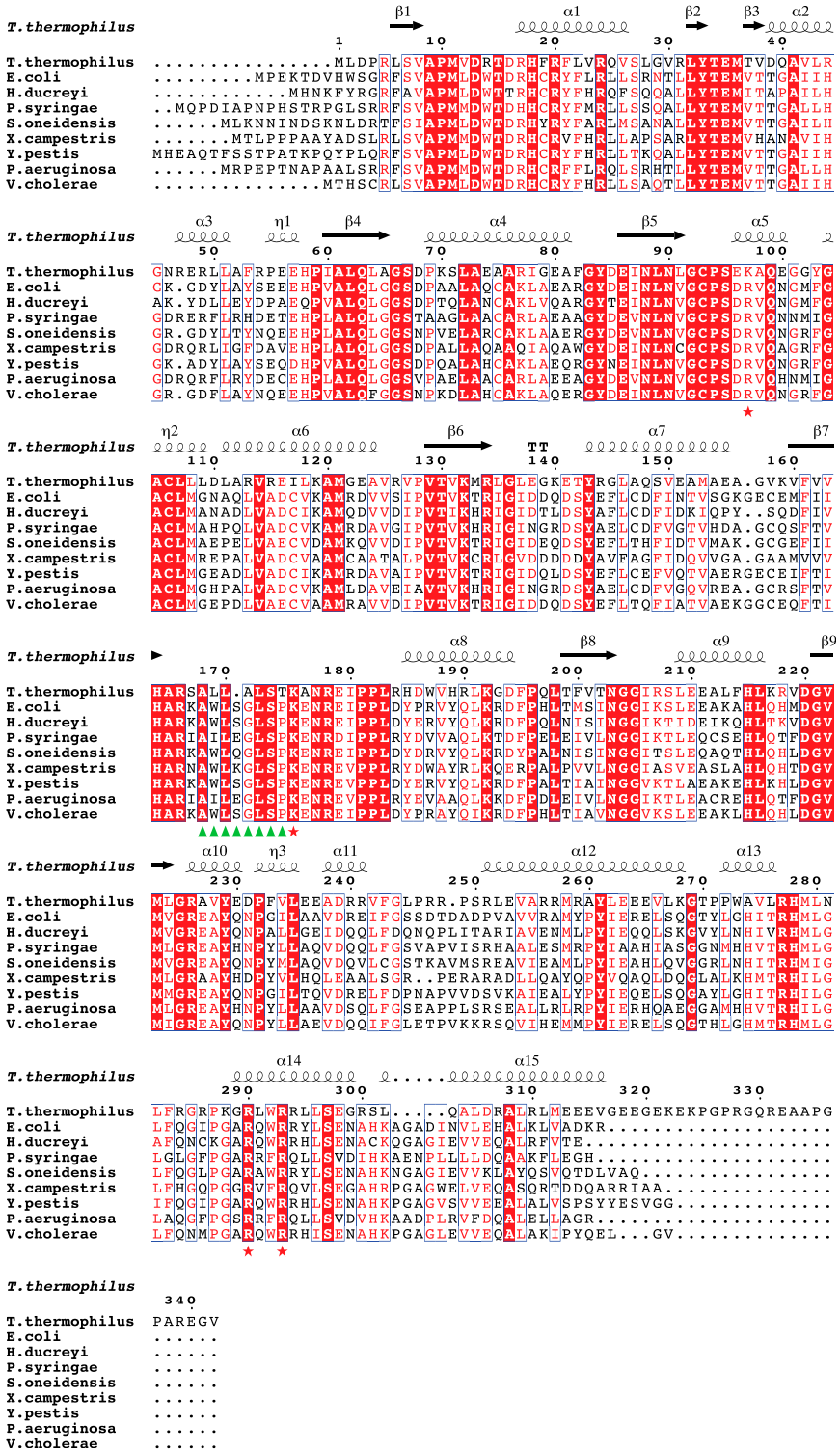

Fig. S7. Sequence alignment of DusA subfamily enzymes with 30–50% sequence identity. Residues that are proposed to define tRNA docking (binding signatures) are highlighted by red stars. The conserved eight-residue insertion, preceding Lys175, is highlighted by green triangles.

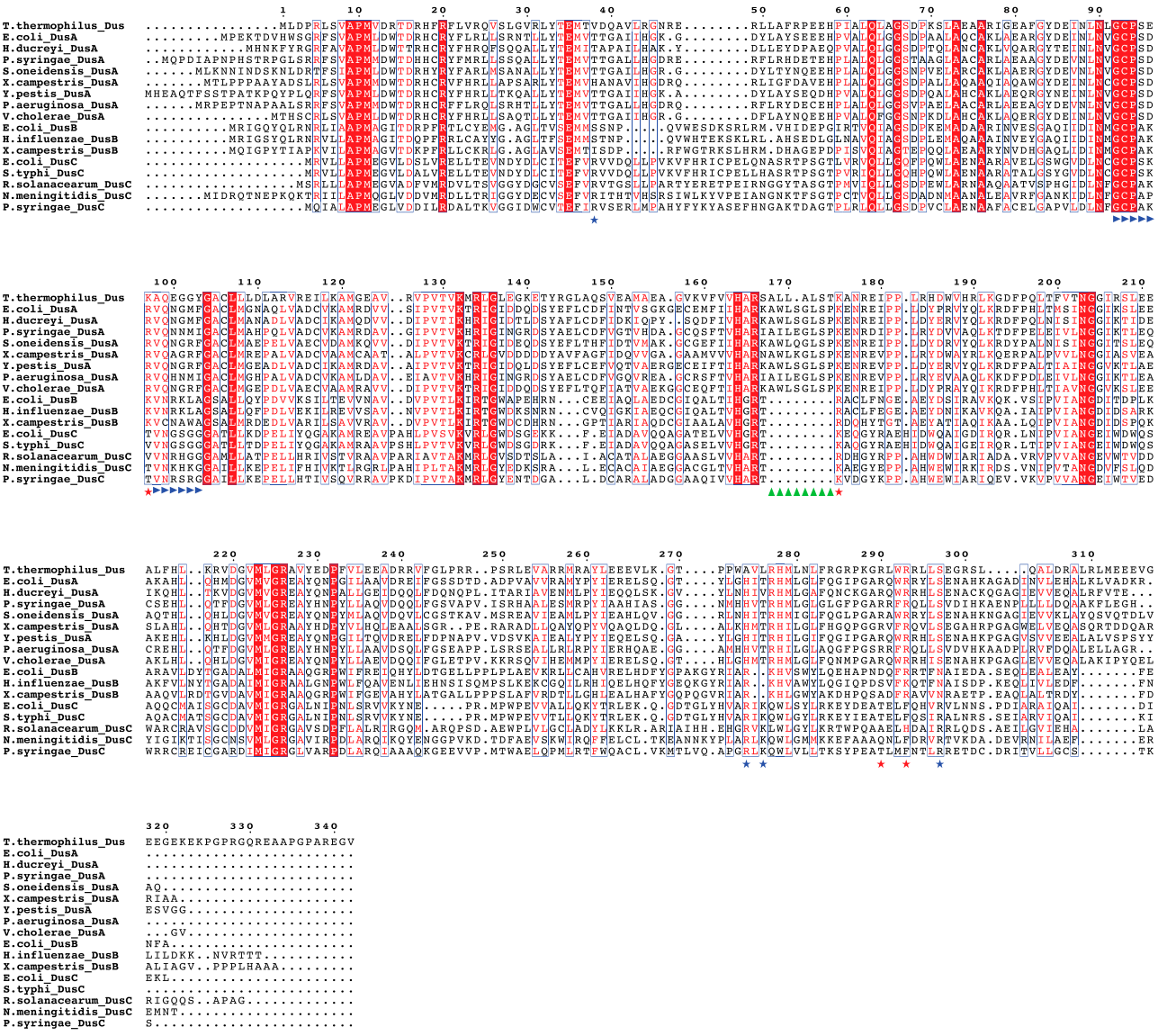

Fig. S8. Sequence alignment of Dus enzymes from subfamilies DusA, DusB, and DusC showing conservation (red background, white letters) and similarity (red letters). Residues constituting the proposed DusC and DusA binding signatures are highlighted by blue and red stars, respectively. The flexible loop of DusC is indicated by blue arrows. The conserved eight-residue sequence insertion of DusA is highlighted by green triangles.

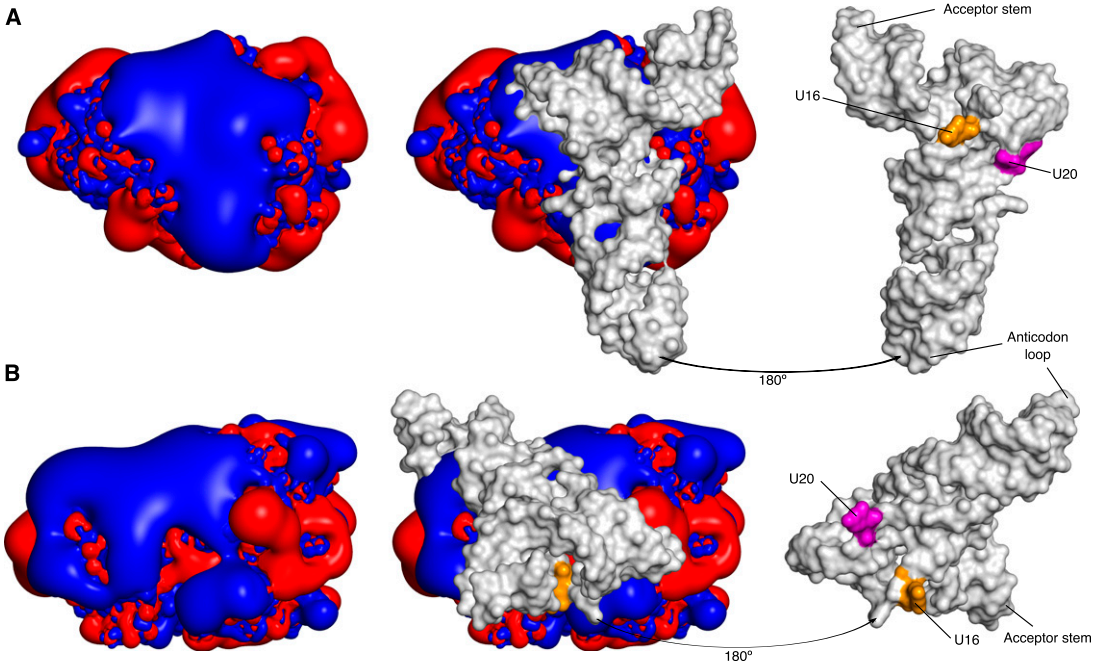

Fig. S9. tRNA binding in reverse orientations. (*A*) DusC. (*B*) *Tt*Dus. Images on the *Left* show proteins' electrostatic isosurfaces contoured at ± 1 kTe^{-1} (blue/red). Protein–tRNA complex formation (*Center* and *Right*) is shown with U16 (orange) and U20 (pink) highlighted on tRNA surfaces. tRNA (*Right*) is rotated by 180° with respect to the center image.